Droplet Impact and Wetting on a Micropillared Surface

Yagya Narayan and Rajneesh Bhardwaj

1 Introduction

Superhydrophobic surfaces engineered with micro/nano features are ubiquitous due to their important properties like self-cleaning [1, 2], anti-icing [3], and dropwise condensation [4]. In general, the surface morphology is bioinspired by nature; for instance, taro [5] and lotus leaves [6] that possess self-cleaning properties. These properties can influence the droplet wetting and impact behaviour with substrate, and may result in slippery and low hysteresis surfaces [7–10].

A microtextured surface is fabricated by developing grooves/pillars by physical or chemical processes [5, 11]; wherein the characteristics are defined on the basis of surface height correlations. A droplet spreads and settles on a surface in a metastable configuration based on the degree of wettability for a given solid–liquid system [12]. A droplet on physically textured surfaces principally has two states, that is, Wenzel and Cassie state. In Wenzel state, the wetting front follows all the topographical variations of surface. Minimum energy required to form unit area solid–liquid interface by replacing its solid–vapour interface component, yields the following equation for the contact angle [13, 14];

$$\cos\theta_r^w = r\cos\theta_e \tag{1}$$

where r is the roughness factor, the ratio of the actual liquid–solid contact area to the total projected area. In the case of Cassie state, the droplet only wets the top area of pillars and thus forming a void space between them. The energy minimization process provides an expression for contact angle as follows [13, 14];

$$\cos\theta_r^c = \phi_s\cos\theta_e + \phi_s - 1 \tag{2}$$

Y. Narayan · R. Bhardwaj (✉)
Department of Mechanical Engineering, IIT Bombay, Mumbai 400076, India
e-mail: Rajneesh.bhardwaj@iitb.ac.in

K. M. Singh et al. (eds.), *Fluid Mechanics and Fluid Power, Volume 5*, Lecture Notes in Mechanical Engineering, https://doi.org/10.1007/978-981-99-6074-3_12

where ϕ_s is the ratio of liquid–solid contact area (or droplet pillar contact area) to the total projected area.

Numerous studies [15, 16] have demonstrated the effects of elasticity [17], roughness [18] and physicochemical properties of surfaces [19, 20]. In the context of droplet impact, impact on micro-textured surface provides different regimes such as complete rebound, partial rebound, and no-rebound [20], and effects like droplet splashing [18], spreading, receding and bouncing [21] on interaction with substrate. A droplet acquires kinetic energy over the height of the fall, which gets converted into surface energy and loses in the form of viscous dissipation/heat generation. The interplay of energies decides the bouncing and non-bouncing behaviour (see Patil et al. [20] and review by Yarin [21]). Extensive research has been done on droplet-bouncing and non-bouncing surfaces with hydrophobic and superhydrophobic properties. The deformation in the droplet's shape on impact [22, 23] and comparison to its impact on hydrophilic surfaces have also been reported [24]. Patil el al. [20] studied the droplet impact on a micro-textured surface with square pillars arranged in a square arrangement and three regimes, namely partial bouncing, complete bouncing, and non-bouncing were reported.

A brief literature review shows that there are several open research questions. For instance, do wetting characteristics change if micropillars are arranged in two different profiles with equal liquid–solid contact area fraction ϕ_s? Does Weber number at which droplet starts to change its wetting behaviour from Cassie state depends on the arrangement of pillars?

To this end, the objective of this paper is to measure contact angle and droplet wetting diameter on a microtextured surface with two different pillar arrangements and to analyse droplet impact on each surface. The ratio of liquid–solid contact area to the total projected area has been kept constant, as shown in Fig. 1.

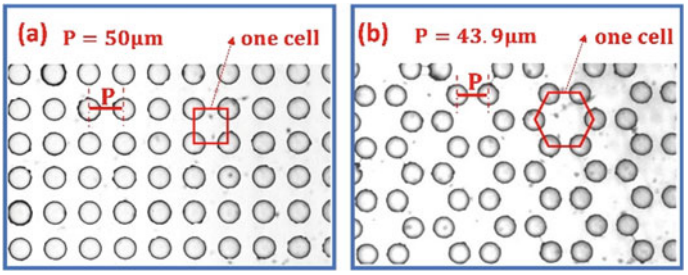

Fig. 1 Optical microscopic image of pillars arranged in (**a**) square profile, (**b**) hexagon profile. The profile of one cell and corresponding pitch lengths have been illustrated

2 Methodology

In this work, micro-textured surfaces were manufactured by standard photolithography techniques. Five sets of surfaces were manufactured with the same liquid–solid contact area fraction ϕ_s in each set. The characteristic distance defining a single cell is called pitch. Figure 1 shows one set of surfaces; a surface with pillars arranged in square profile (a) on the left and with hexagonal profile (b) on the right side. We consider square and hexagonal profile of pitch distance l and a, respectively. The relation between these distances can be found by equating ϕ_s for both surfaces (considering one cell), as follows;

$$\frac{\pi r_p^2}{l^2} = \frac{2\pi r_p^2}{\frac{3\sqrt{3}a^2}{2}}, \tag{3}$$

where r_p is the radius of the pillar. The only variable in the expression used by Patankar (Eq. 2) is ϕ_s (equilibrium contact angle is taken as a constant). According to this equation, the contact angle value for surfaces with equal ϕ_s are the same. However, this expression does not account for pillar arrangement and concludes that the droplet's shape is the same for different pillar arrangements. The relation between l and a for equal ϕ_s can be written as follows;

$$a = \frac{2l}{3\sqrt{3}}. \tag{4}$$

The total number of cells involved can be calculated by dividing the total wetted area πR^2 by the area of a single cell. The areas of a cell are l^2 and $\frac{3\sqrt{3}a^2}{2}$ in the case of square and hexagonal profiles, respectively.

2.1 Fabrication Process for Making Micropillared Surfaces

The standard photolithography technique was used for the fabrication of micropillared surfaces. The polished side of a 2-inch Si wafer was spin-coated with SU-8 2025 epoxy photoresist polymer. Firstly, Si wafer was RCA cleaned and placed in a furnace for wet oxidation to remove suspended particles and prevent soluble components at a later stage. Secondly, the wafer was spin-coated at 500 rpm for 10 s, followed by 2300 rpm for 40 s. Thirdly, the wafer was gently baked for 3 min at 65^o C followed by 8 min at 95^o C. A double-sided aligner (EVG620, EV Group Inc.) was used to align the iron oxide coated glass mask with square-shaped patterns using a Laser Writer (LW405, Microtech Inc.). Additionally, the wafer was subjected to UV light for two to three minutes at an intensity of 160 mJ/cm^2. Fourthly, the post-baking procedure includes heating at 65^o C for 1 min and 95^o C for the next 6 min, followed by atmosphere cooling at ambient temperature. After that, samples were cleaned with

isopropanol and processed for 5–6 min in SU-8 photo developer. Finally, the hard baking step includes 10-min baking at 120^o C. These surfaces were coated with 10 nm Pt coating for comparison with previously published data [20] and increasing durability of surfaces. Optical images of surfaces were taken using an optical microscope (Olympus MX-40, objective lens 4X); representative surfaces with pitch distance of 50 and 43.9 μm for square and hexagonal profiles, respectively (Fig. 1), for all the surfaces diameter of pillars is 20 μm. The error in diameter and pitch distance are ± 1 μm and ± 2 μm, respectively, which is used for error bars in the result section.

The pitch distances taken for the square profile are 40, 50, 60, 70, and 80 μm. For hexagonal arrangements, the corresponding values are 35, 43.9, 52.6, 61.4, and 70.2 μm. Each surface's pillar diameter is constant, that is 20 μm. Figure 1 shows optical microscopic images of pillars arranged in (a) square profile and (b) hexagon profile with the same solid area fraction. A red polygon indicates the geometry of one cell in each part of the figure, which differs in two cases.

2.2 Generation and High-Speed Visualization of a Droplet

Figure 2 shows the setup for (a) visualization of droplet behaviour on the surface and (b) high-speed imaging of droplet impact on the surface of interest. A deionized water droplet of diameter 1.7 ± 0.05 mm, generated using a 31 gauge needle syringe (BD Inc.), was used for experiments. Isopropanol liquid was used for cleaning surfaces. After drying out, the impact was analysed with a high-speed camera (NXA3S3 IDT Inc.), assembled with a microscopic objective lens (Qioptiq Inc.) having a focal length of 9.5 cm. This phenomenon was recorded at 1000 frames per second (fps) to ensure sufficient frames for all information about the phenomenon. Required velocities are generated via droplets falling under gravity. The difference between the surface and the needle tip height varied from 2 to 15 mm. This height adjustment is ensured by a height-adjustable precision table (Holmarc Inc.). The velocity thus obtained varies from 0.14 to 0.54 m/s, corresponding to the Weber number from 0.46 to 6.885. Images were rendered and analysed using *ImageJ* software to measure contact angle and wetted diameter. The angle between the surface and the tangent to the droplet at the three-phase contact point is analysed and reported as the contact angle (as shown in Fig. 3). The contact angle of the flat surface comes out to be 92^o. The contact angle and wetted diameter uncertainty are ± 2° and ± 0.03 mm, respectively. To ensure repeatability, experiments were repeated at least three times.

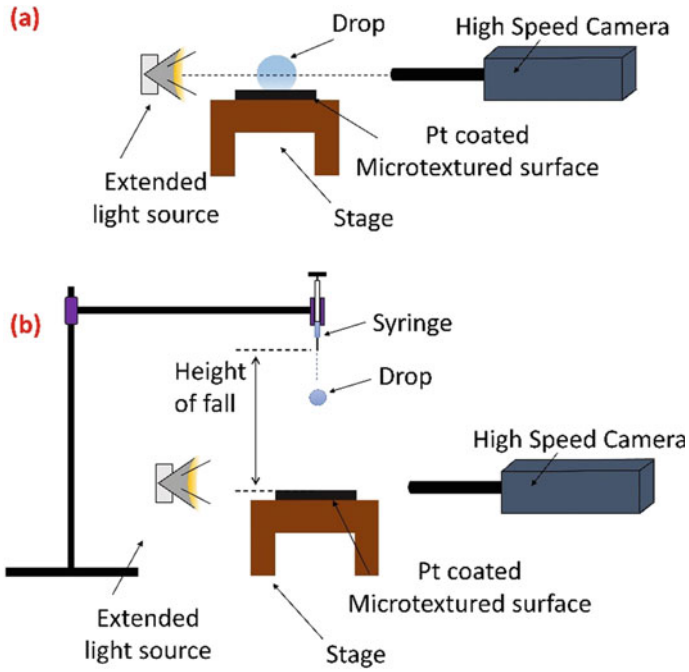

Fig. 2 Experimental set-up depicting components used for: (**a**) droplet behaviour visualization (**b**) impact visualization

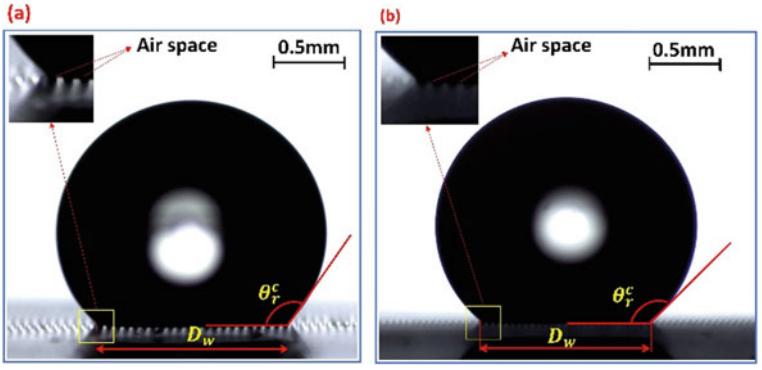

Fig. 3 Contact angle and wetted diameter comparison between pillars arranged in (**a**) square profile with pitch 60 μm and (**b**) hexagonal profile with pitch 52.4 μm. Zoomed view of contact line, which shows air space between pillars of the microtextured surface, is also shown on the left-top of each part. In case of square profile, air space is clearly visible, however, due to positioning of pillars in hexagon, only light coming from beyond is visible

3 Results and Discussion

3.1 Wetting Characteristics

Figure 3 illustrates droplet characteristics over square profile (a) with pitch 60 μm, and hexagonal profile (b) of pitch 52.4 μm. The two test cases has an equal value of liquid–solid contact area fraction ϕ_s. On the left-top side of each part, a zoomed-in view of the three-phase contact point is added, which depicts air space between pillars, confirming the presence of Cassie state. The contact angle on the two surfaces are almost same.

Figure 4 illustrates values of contact angle and wetted diameter as a function of liquid–solid contact area fraction for pillars arranged in square and hexagonal profiles. On decreasing ϕ_s from 0.2 to 0.05, the contact angle increases for square profiles from 93^o to 141^o. Similarly, droplets on hexagonal profiles follow the same trend, but at $\phi_s = 0.05$, the droplet on square profiles exhibits the Wenzel state. In contrast, the value of contact angle at this ϕ_s, for hexagonal profiles is larger, implying Cassie state. The theoretical trend plotted with experimental data confirms this hypothesis. The corresponding values of wetted diameter are also shown. The sharp jump at $\phi_s = 0.05$ indicates the Wenzel condition, which means Cassie state does not exist at and beyond this ϕ_s for the square profile.

3.2 Effect of Weber Number for Non-bouncing Condition

Further, we performed droplet impact experiments on the two profiles. Figure 5 shows a comparison of the Weber number (We) for the two profiles at which the impacting droplet does not bounce. Beyond this Weber number, either the droplet shows partial bouncing leaving a satellite droplet on the surface or it directly enters into the Wenzel state. Below this Weber number, the droplet always bounces on the surface. In all cases, hexagonal structure shows a larger We than square structure. The value of We is significantly larger at the largest pitch (or lowest ϕ_s). In this case, the droplets go to the Wenzel state in square structure, however, it does not in case of hexagonal profile.

4 Conclusions

In conclusion, the present study provides fundamental insights into the wetting characteristics of micro-textured surfaces when the arrangement of pillars is modified. A regular hexagon possesses general characteristics because a circle can be closely approximated into a hexagon, incorporating all the available substrate area. We analysed droplet contact angle and wetting diameter concerning the arrangement of

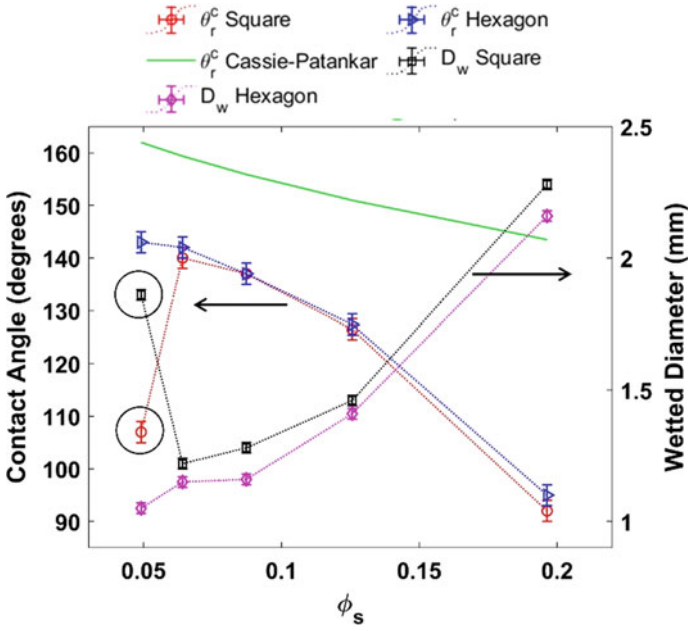

Fig. 4 Comparison of theoretical and experimental values of contact angle in square and hexagonal arrangement (y-axis left) is shown. A comparison of wetted diameter between square and hexagonal arrangement (y-axis right) is shown. Values of theoretical contact angle is adopted from Patankar [13]. Points depicted by circles indicate experimental Wenzel states

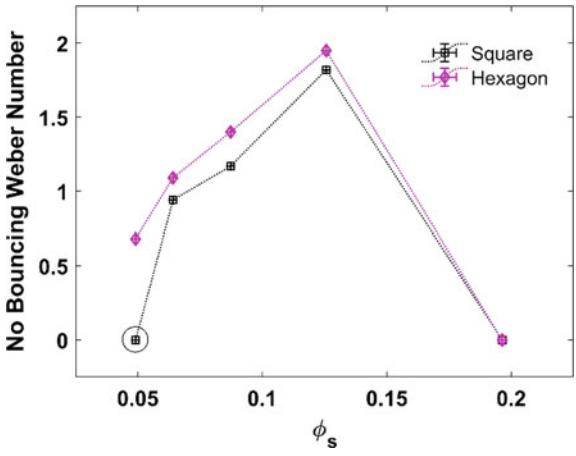

Fig. 5 Comparison of points when droplet does not bounce completely and transits into Wenzel state afterward. Points depicted by circles are Wenzel states

pillars, that is, when pillars are arranged in square and hexagon profiles. These pillars were manufactured by standard photolithography. The hexagonal profile shows better results than the square profile by continuing into Cassie state at lower ϕ_s, when the square arrangement fails to do so. The contact angle and wetted diameter in both cases are almost the same; however, the droplet exhibits the Wenzel state at high pitch distances (or low ϕ_s) in the case of square arrangement.

Nomenclature

r	Roughness factor
ϕ_s	Liquid–solid contact area fraction
θ_e	Equilibrium contact angle at flat surface [rad]
θ_r^w	Contact angle in case of Wenzel state [rad]
θ_r^c	Contact angle in case of Cassie state [rad]
r_p	Radius of micropillar [μm]
R	Wetting radius of a droplet [μm]
l	Pitch distance in case of square profile [μm]
a	Pitch distance in case of hexagonal profile [μm]

References

1. Blossey R (2003) Self-cleaning surfaces—virtual realities. Nat Mater 2(5):301–306
2. Nishimoto S, Bhushan B (2013) Bioinspired self-cleaning surfaces with superhydrophobicity, superoleophobicity, and superhydrophilicity. RSC Adv 3(3):671–690
3. Liu K, Jiang L (2012) Bio-inspired self-cleaning surfaces. Annu Rev Mater Res 42:231–263
4. Xuemei C, Jun W, Ruiyuan M, Meng H, Nikhil K, Shuhuai Y, Zuankai W (2011) Nanograssed micropyramidal architectures for continuous dropwise condensation. Adv Funct Mater 21(24):4617–4623
5. Kumar M, Bhardwaj R (2020) Wetting characteristics of colocasia esculenta (taro) leaf and a bioinspired surface thereof. Sci Rep 10(1):1–15
6. Zhang M, Feng S, Wang L, Zheng Y (2016) Lotus effect in wetting and self-cleaning. Biotribology 5:31–43
7. Martin V, Yuxi Z, Noor AJ, Leyla S, Tohid FD (2019) Liquid-infused surfaces: a review of theory, design, and applications. Acs Nano 13(8):8517–8536
8. Bruno A, Jacco HS (2020) Statics and dynamics of soft wetting. Ann Rev Fluid Mech 52:285–308
9. Laxman KM, Nagesh DP, Rajneesh B, Adrian N (2017) Droplet bouncing and breakup during impact on a microgrooved surface. Langmuir 33(38):9620–9631
10. Manish K, Rajneesh B, Kirti Chandra S (2020) Wetting dynamics of a water droplet on micropillar surfaces with radially varying pitches. Langmuir 36(19):5312–5323
11. Lena A, Kari M, Mika S (2020) Precise fabrication of microtextured stainless steel surfaces using metal injection moulding. Prec Eng 62:89–94
12. Abraham M, Claudio DV, Stefano S, Alidad A, Jaroslaw WD (2017) Contact angles and wettability: towards common and accurate terminology. Surf Innov 5(1):3–8

13. Neelesh AP (2003) On the modeling of hydrophobic contact angles on rough surfaces. Langmuir 19(4):1249–1253
14. David Q (2008) Wetting and roughness. Ann Rev Mater Res 38(1):71–99
15. Christophe J, Sigurdur TT (2016) Drop impact on a solid surface. Ann Rev Fluid Mech 48(1):365–391
16. Khojasteh D, Kazerooni M, Salarian S, Kamali R (2016) Droplet impact on superhydrophobic surfaces: a review of recent developments. J Ind Eng Chem 42:1–14
17. Hardt S, McHale G (2022) Flow and drop transport along liquid-infused surfaces. Annu Rev Fluid Mech 54:83–104
18. Hao J (2017) Effect of surface roughness on droplet splashing. Phys Fluids 29(12):122105
19. Chenlu Q, Fan Z, Ting W, Qiang L, Dinghua H, Xuemei C, Zuankai W (2022) Pancake jumping of sessile droplets. Adv Sci 9(7):2103834
20. Nagesh DP, Rajneesh B, Atul S (2016) Droplet impact dynamics on micropillared hydrophobic surfaces. Experiment Therm Fluid Sci 74:195–206
21. Alexander LY et al (2006) Drop impact dynamics: splashing, spreading, receding, bouncing. Ann Rev Fluid Mech 38(1):159–192
22. Christophe C, C´edric B, Denis R, David Q (2004) Maximal deformation of an impacting drop. J Fluid Mech 517:199–208
23. Li X, Mao L, Ma X (2013) Dynamic behavior of water droplet impact on microtextured surfaces: the effect of geometrical parameters on anisotropic wetting and the maximum spreading diameter. Langmuir 29(4):1129–1138
24. Antonini C, Amirfazli A, Marengo M (2012) Drop impact and wettability: from hydrophilic to superhydrophobic surfaces. Phys Fluids 24(10):102104